ISSN 1070-3632, Russian Journal of General Chemistry, 2012, Vol. 82, No. 12, pp. 2070–2078. © Pleiades Publishing, Ltd., 2012.
Original Russian Text © A.R. Dubrovskii, S.A. Kuznetsov, E.V. Rebrov, J.C. Schouten, 2011, published in Rossiiskii Khimicheskii Zhurnal, 2011, Vol. 55, No. 2, pp. 43–51.

Catalysts of New Generation and Microstructured Heat-Exchanger Reactors for the Water–Gas Shift Reaction

A. R. Dubrovskii[a], S. A. Kuznetsov[a], E. V. Rebrov[b], and J. C. Schouten[c]

[a] *Tananev Institute of Chemistry and Technology of Rare Elements and Mineral Raw Materials, Karelian Branch, Kola Research Center, Russian Academy of Sciences, Akademgorodok 26a, Apatity, 184209 Russia*
e-mail: kuznet@chemy.kolasc.net.ru

[b] *School of Chemistry and Chemical Engineering, Belfast, United Kingdom*
e-mail: e.rebrov@qub.ac.uk

[c] *Eindhoven University of Technology, Den Dolech 2, Eindhoven, 5600 MB the Netherlands*
e-mail: j.c.schouten@tue.nl

Received May 5, 2011

Abstract—The catalytic systems of new generation and microstuctured heat-exchanger reactors for the water–gas shift reaction have been considered.

DOI: 10.1134/S1070363212120274

INTRODUCTION

Microstructured reactors are miniature systems for performing reactions, fabricated by microengineering or fine machining techniques [1]. As a rule, microreactors contain channels 10–500 μm in diameter, due to which a fairly high surface area-to-internal volume ratio (10000–50000 m^2/m^3; the respective value in conventional reactors is about 100 and, very rarely, 1000 m^2/m^3) and high rates of heat and mass transfer can be reached [2, 3].

Microstructured devices were first reported in 1989 [4]. At the conference on the microsystem engineering of chemical and biological reactors in Germany in 1995 [5], microreactor engineering was recognized as a new branch of science. Since then this subject area has vigorously progressed, and its achievements are reflected in the reviews [1, 6–8].

Processes in microchannels involve intense heat and mass transfer. The heat flux density in microchannels is as high as 20000–35000 W m^{-2}, which is higher by an order of magnitude compared to conventional systems; the mass-transfer coefficient varies within the range 5–15 s^{-1}, whereas in fixed-bed reactors it is 0.01–0.08 s^{-1}. Therefore, the reaction rates and, consequently, process efficiency in microreactors are higher than in traditional reactors [9]. Moreover, microreactors make it possible to solve the problems of nonuniform temperatures (in the case of highly exothermal reactions [10–12]) or nonuniform concentrations (when reagents are mixed in the reactor [13, 14]), which favors higher reaction selectivities and yields. Microreactors are suitable for measuring reaction rates, since the working temperatures in them are constant or uniform [11, 15].

Using microreactors as a measurement and computational equipment reduces power and material consumption, and the high thermal conductivity and mass transfer reduce computation or analysis time [16]. The above-mentioned advantages explain a great interest in microreactors and development of experimental production of this equipment [17, 18]. Owing to their small size, microreactors allow safe operation with dangerous chemical reagents [19], and flame-arresting properties of microchannels provide explosive safety in the operation with mixtures in the reagent auto-ignition region [20, 21]. It has become possible to perform reactions in previously inaccessible conditions and thus increase reaction selectivity and yield and decrease reagent consumption.

Another characteristic advantage of microreactors consists in their modular construction. The customer obtains ready modules with all necessary engineering equipment and assembles the reactor by the Lego

principle. Moreover, if necessary the processing chain can be disassembled to replace the catalytic microreactor by a fresh one. This approach is usually practiced in fine organic synthesis, where most reactions are performed in batch reactors, as well as in hydrogen power engineering, where rapid transition from one fuel to another is required.

Moreover, the modular construction of microreactors allows a more decentralized industry and on-site preparation of reagents (sometimes dangerous). In this case, transportation risks are excluded, and transportation costs are reduced [22, 23].

Along with the above-mentioned advantages, microreactors have a number of drawbacks. In view of the short reagent residence times (from milliseconds to seconds), microreactors are less suitable for slow reactions [24]. Furthermore, microreactors are fairly expensive instruments, and the replacement of one big reactor by a large number of small ones [6] adversely affects production efficiency. Microreactors are sensitive to erosion and corrosion [5]. In addition, pure reagents should be used to prevent microchannel clogging [25].

There are several features which distinguish microreactors from conventional ones and are very important for mathematical reactor simulation [8]. Reactor simulation is an important aspect of chemical engineering, since it underlies design and optimization of chemical engineering equipment. Since the fluid flow in microreactors is usually laminar, the models of microreactors are more precise compared to traditional reactors, and this gives grounds to suggest that microreactors are potentially more reliable in operation. The main differences between microreactors and large-scale equipment are the following: (a) the flows in microstructured reactors are laminar, whereas in macroreactors they are mostly turbulent; (b) the rates of heat and mass transfer in microreactors are very high, whereas in macroreactors these rates are the limiting factor; (c) solid-phase thermal conductivity is an important factor in microreactors and not so important in traditional reactors; (d) small-sized reactors are more sensitive to the environment than large-sized ones; and (e) since microreactors have high surface area-to-volume ratios, surface effects in them are much more important than in macroreactors.

Now microtechnologies are the most widely applied in fine organic synthesis [27–29].

In the present paper we consider state-of-the-art catalytic systems and constructions of microstructured reactors/heat-exchangers for the water-to-gas shift reaction. This reaction was chosen, because the microchannel reactors and the catalysts for hydrogen production from methanol, ammonia oxidation, partial hydrocarbon oxidation, and others have been fairly well documented [30–33].

Catalytic Systems of New Generation for the Water-Gas Shift Reaction

The water–gas shift reaction is one of the key stages of hydrogen production from gaseous, liquid, and solid hydrocarbons and alcohols. This reaction is used to success in the gas industry for hydrogen and syngas production [34, 35]. In proton-exchange membrane fuel cells, there is a high probability of platinum poisoning with carbon monoxide on the anodic catalyst. Thorough removal of CO to a level of a few ppm is required. On the other hand, the activity of existing commercial catalysts for the water–gas shift reaction is usually not too high, and the large part of the fuel processor for hydrogen production is occupied by the reacting system. Synthesis of more active and stable catalysts is urgent to improve the efficiency of the water–gas shift reaction in fuel processing.

The water–gas shift reaction

$$CO + H_2O \rightleftarrows CO_2 + H_2$$

is reversible and exothermic (ΔH^0_{298} –41.1 kJ mol^{-1} at the STP). The highest equilibrium conversion of CO is reached at low temperatures, and, therefore, the water–gas shift reaction is accomplished in two stages: high-temperature (catalyst Fe_3O_4/Cr_2O_3) and low-temperature (catalyst $CuO/ZnO/Al_2O_3$).

In what follows we discuss the state of the art in the development of high-temperature and low-temperature catalysts for the water–gas shift reaction.

Methods of Catalyst Arrangement

In microreactors, catalysts are most frequently arranged in two ways: (1) by packing submillimeter channels with fine catalysts granules [36] and (2) by fixing catalysts on channel walls. The hydrodynamic resistance in the first-type microreactors is much higher.

Much more promising are the second-type microreactors which contain more than 10000 channels 50–1000 μm in diameter and 20–100 mm in length. Owing to short residence times, these reactors have a high

specific performance, and the volume rate of the gas mixture is ~100 $cm^3 s^{-1}$. The techniques for fixation of catalysts on channel walls and the application fields of microreactors are considered in the monographs [1, 8, 37] and reviews [38, 39].

High-Temperature Water-Gas Shift Catalysts

The conventional commercial high-temperature water–gas shift catalyst is a mixed iron–chromium oxide, working range 310–480°C. This catalyst shows a satisfactory activity and an excellent thermal stability, since the activator (chromium) acts as structure stabilizer and/or structure activator. Commercial catalysts also offer the advantages of low cost, high durability, and sulfur resistance.

Attempts to promote the Fe_3O_4/Cr_2O_3 catalyst by alloying the iron and chromium oxides were undertaken. Efficiency of small CuO, CoO, and ZnO additions to this catalyst was studied [40]. Edwards et al. [41] alloyed the catalyst by first-row transition metal oxides. Rhodes et al. [42] tried to promote Fe_3O_4/Cr_2O_3 by co-precipitation with 2 wt % of B, Cu, Ba, Pb, Hg, and Ag. It was found that boron slightly decreases activity, while the other elements increase it in the series

Hg > Ag, Ba > Cu > Pb > unpromoted catalyst > B.

Copper as an active promoter was expected to be distributed in the catalyst as a solid solution but was found to be present segregated on the surface. This finding gives grounds to suggest that, according to data on a promoted lead catalyst [43], copper most likely provides electronic activation of Fe_3O_4/Cr_2O_3 than forms new active centers in the oxide matrix. Lei et al. [44] found that the water–gas shift reaction can be much accelerated by doping a little of Rh in Fe_3O_4/Cr_2O_3.

Commercial iron-based catalysts containing 8–14 wt % of Cr (contains ~2 wt % of Cr^{+6}) are very toxic, and, therefore, attempts were made to develop a chromium-free iron catalyst, while not sacrificing activity and thermal stability. Different oxides were tested, specifically PbO, La_2O_3, CaO, ZrO_2, and Al_2O_3, as Cr_2O_3 substitutes, but the resulting catalysts showed quite a low activity. Liu et al. [45] prepared an iron catalyst promoted with Ce and Al oxides and found it no less active and thermally stable as commercial Fe_3O_4/Cr_2O_3.

Low-Temperature Water-Gas Shift Catalysts

The standard low-temperature water–gas shift catalyst is $Cu/ZnO/Al_2O_3$ works in the temperature range 160–250°C in air. At 300°C it undergoes auto-ignition. Moreover, this catalyst is deactivated on thermal caking and on contact with water, sulfur, and halides.

To go around these drawbacks, other types of catalysts for low-temperature steam conversion are being studied, in particular, noble metals deposited on reduced metal oxides. Over the past years much interest has arisen in gold-containing catalytic systems. Haruta [46] showed that the catalysts containing gold nanoparticles exhibit quite a high activity if deposited on an appropriately pretreated support. The enhancement of the catalytic activity is due to interaction of gold nanoparticles with the support. The key issue here is the construction of the gold–support interface [44].

Burke and Nugent [47] found that clusters of extremely small gold particles exhibit unusual properties, namely, they are able to coordinate much more oxygens and/or hydroxyls, which opens the way to their successful use in oxidation reactions. Analysis of published evidence on the application of gold-containing catalysts [48] revealed an important role of the support and its pretreatment for preparing highly dispersed gold particles on the support and, consequently, providing a strong gold–support interaction.

Andreeva [49] noted that important for a high activity and stability of gold catalysts for water–gas shift reactions is the choice for each specific process of a support best interacting with gold and the high degree of dispersion of gold particles on the support surface. The optimum size of gold particles, providing a uniform distribution of gold particles on the support surface and a high catalyst activity, is 3–5 nm.

In the long run, the choice of high-activity catalysts is critically dependent on the knowledge of various mechanistic aspects of the reaction. The catalytic activity of oxides of transition metals, including gold, is qualitatively estimated as follows: $Au/Fe_2O_3 \cong Au/TiO_2 \cong Au/ZrO_2 > Au/Co_3O_4$.

Platinum was also studied as a promoter of catalysts on the basis of transition metal oxides. Ricote et al. [50] managed to drive the water–gas shift reaction using a zirconia-doped cerium oxide to prepare a platinum-promoted Ce_2O_3/ZrO_2 binary oxide catalyst. Iida and Igarashi [51] established that the reactivity of adsorbed carbon monoxide toward steam is enhanced by doping rhenium in the Pt/ZrO_2 and Pt/TiO_2 catalysts.

Molybdenum carbide with a high specific surface area is presently being explored as a potential catalyst for the water–gas shift reaction. This material exhibits a high catalytic activity in various reactions, an exceptionally high thermal and chemical stability, and a high resistance to sulfur poisoning. Transition metal carbides are close in catalytic properties to noble metals which, as mentioned above, are excellent catalysts for the water–gas shift reaction. An important advantage of molybdenum carbide is that it is much cheaper than noble metals. Patt et al. [52] showed that molybdenum carbide Mo_2C was catalytically more active than the commercial catalyst $Cu/ZnO/Al_2O_3$ in the water–gas shift reaction performed at 220–295°C at atmospheric pressure; moreover, molybdenum carbide did not catalyze the methanation reaction. Further evidence for a higher catalytic activity and stability of Mo_2C compared to $Cu/ZnO/Al_2O_3$ was obtained in [53–58]. The principal method of synthesis of molybdenum carbide on a molybdenum support is the oxidation of molybdenum plates under a dry air flow at a volume rate of 50 ml min^{-1} at 400°C for 16 h. In the presence of oxygen at temperatures above 350°C, molybdenum is oxidized to an orthorhombic oxide MoO_3 which is thermodynamically most stable under these conditions [59] and can be reduced to a hexagonal carbide Mo_2C (cubic Mo_2C content <10 wt %) in hydrogen containing 20 vol % of methane under gradual heating to 700°C with hold-up at that temperature for 30 min [55].

Electrochemical synthesis of molybdenum carbides in molten salts offers a number of advantages. For example, pulse- and pulse-reverse-current electrodeposition techniques allow one to control the structure, thickness, porosity, roughness, and texture of galvanic deposits and their grain size (up to nano sizes). Other advantages include the following: (a) the synthesis temperature is fairly low (700–900°C); (b) lab-scale electrodeposition parameters can be transferred to a large-scale process and also adapted for processes on complex-shaped supports without sacrificing the grain size and coating composition; (c) the resulting coating are quite pure, even if low-quality starting materials are used; and (d) the operating expenses are low and the electrochemical equipment is inexpensive.

The electrochemical synthesis of molybdenum carbide coatings on a molybdenum support in [60–62] was performed by galvanostatic electrolysis of molten $NaCl–KCl–Li_2CO_3$, $NaCl–KCl–Li_2CO_3–Na_2MoO_4$, and $LiCl–KCl–Li_2C_2$ salts (systems 1, 2, and 3, respectively). In systems 1 and 3, molybdenum carbide was formed from a molybdenum support and carbon generated by ion-arc discharge. The conditions of Mo_2C synthesis on molybdenum plates were as follows: temperature 850°C, electrolysis time 7 h, cathodic current density 5 mA cm^{-2} for systems 1 and 2, and anodic current density 5 mA cm^{-2} for system 3. The anode for systems 1 and 2 was a glassy carbon ampule. The thickness of the Mo_2C samples obtained in systems 1 and 3 was no more than 2 μm, since refinery metal carbides form excellent barrier layers and reduce the mutual diffusion coefficients of molybdenum and carbon by several orders of magnitude.

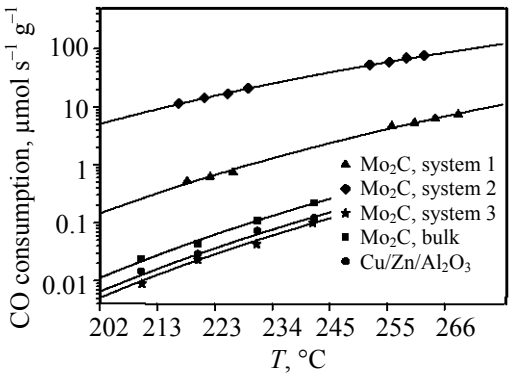

Fig. 1. Temperature dependences of the rate of water–gas shift reactions on various catalysts. Reaction conditions: p_{CO} 0.3 kPa, $p(H_2O)$ 0.76 kPa, $p(CO_2)$ 1.2 kPa, $p(H_2)$ 40 kPa, gas flow rate 50 cm^3 min^{-1} (STP).

Joint electroreduction of MoO_4^{2-} and CO_3^{2-} ions forms 25 μm thick Mo_2C coatings. Morphology, roughness, and specific surface area were determined for Mo_2C samples prepared from different electrolytes and melts of different compositions. In all cases, Mo_2C with a hexagonal lattice was obtained, whereas bulk Mo_2C also contained the a modification (cubic lattice). The presence of cubic M_2C reduces the catalytic activity of the Mo_2C/Mo compositions by 2–3 orders of magnitude and deteriorates its stability. The hexagonal Mo_2C structure is formed due to specific conditions of the electrocrystallization process (electric field, high temperature, etc.).

As seen from the dependence in Fig. 1, the steady-state rates of the water–gas shift reaction in the presence of the Mo_2C/Mo composition synthesized in systems 1 and 2 are higher by one and three orders of magnitude, respectively, that with bulk Mo_2C and commercial $Cu/ZnO/Al_2O_3$ [62]. The steady-state rate of the water–gas shift reaction in the presence of the Mo_2C/Mo

Table 1. Comparative characteristic of catalysts for the water–gas shift reaction[a]

Parameter	$Cu/ZnO/Al_2O_3$	Mo_2C	$Pt, Au/CeO_2$
Activity	+	++	++
Methanation	–	–	>300°C
Pyrophorosity	+	–	–
Stability	+	++	+
Start-up time[b]	–	+	++

[a] (+, ++) Presence and strength of positive characteristics of the catalytic system; (–) lacking or poor characteristics of the catalytic system. [b] Time required to reach the working temperature.

catalyst prepared from system 3 are slightly lower than with the commercial catalyst $Cu/ZnO/Al_2O_3$ because of the thin coating and its low specific surface area. With account for the apparent density and specific surface area of the Mo_2C coatings obtained from varied-composition melts, the activities of the molybdenum carbide samples can be related to the catalyst unit mass. Molybdenum carbide retains stability during many catalytic cycles (more than 5000 h), whereas the activities and reaction surfaces of other catalysts, including those on the basis of noble metals, tend to degrade. With Mo_2C/Mo, no methane formation was observed in the temperature range 250–400°C. The coatings remained stable during cyclic temperature tests, while the commercial catalyst deactivated.

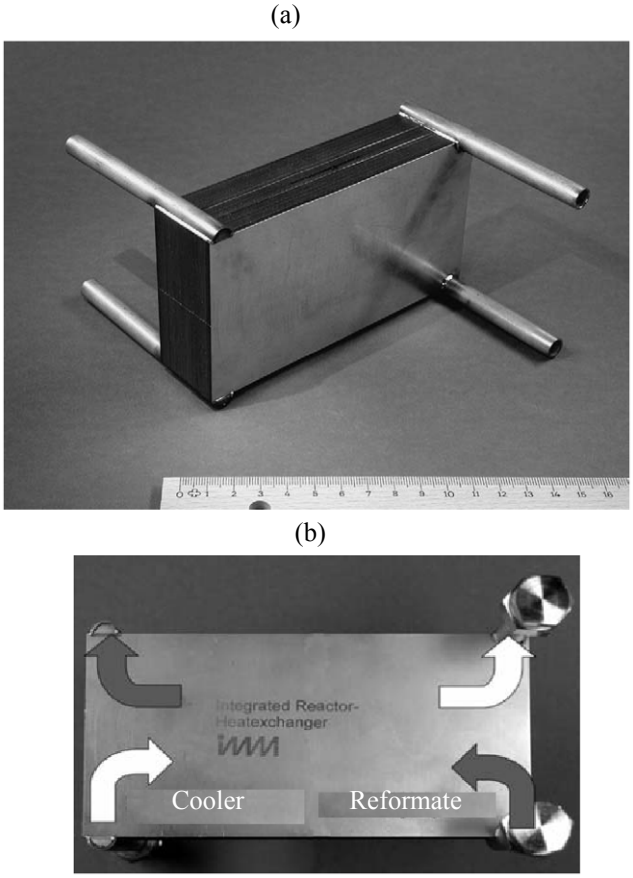

Fig. 2. Integrated microstructured heat-exchanger reactor for the water–gas shift reaction: (a) general view and (b) reac-tion and cooling flow directions.

Comparative characteristic of new-generation molybdenum carbide and noble metal catalysts and the commercial catalyst is presented in Table 1.

Microstructured Heat-Exchanger Reactors for the Water–Gas Shift Reaction

Tonkovich et al. [63] in their research on the feasibility of microreactors for the water–gas shift reaction came to a conclusion that the microstructured reactor for this reaction can be an order-of-magnitude smaller in dimensions than the traditional reactor with a fixed catalyst bed. On the other hand, compared with traditional systems, much more active catalytic coatings are required to carry out the possibility to decrease the dimensions of the reactor by a few orders of magnitude. Goerke et al. [64] developed a microstructured reactor with Ru/ZrO_2 and Au/CeO_2 catalytic coatings. The reactor contains $20\times20\text{-mm}^2$ plates with microchannels 70 μm in depth and 200 μm in width. Note that this reactor is isothermal.

Integrated microstructured reactors/heat-exchangers comprise reactors for high-temperature and low-temperature water–gas shift reactors in a single device. This is provided by creating inside the reactor of a temperature gradient which shifts the thermodynamic equilibrium in a necessary direction [65, 66]. The Mainz Institute of Microtechnology (IMM) developed an integrated microstructured reactor/heat-exchanger (Fig. 2) with a countercurrent cooling system [65]. The necessary temperature gradient is created using the anodic gas of the fuel cell as a cooling medium. Computations showed that a virtually optimal temperature profile can be created by coutercurrent cooling [65]. The next stage involved development of reactor/heat-exchanger heat-exchanger reactor [67, 68] recommended for use as a 5-kW fuel cell (Fig. 3). Reactor consists of 84 stainless-steel plates with etched channels 650 μm and 1000 μm in length. The plates are coated with a $Pt/CeO_2/Al_2O_3$ catalyst bed [69]. The assembly looks like a block 70 mm in height, 214 mm in length, and 139 mm in width, and it contains 7791 microchannels. The weight of the assembly is

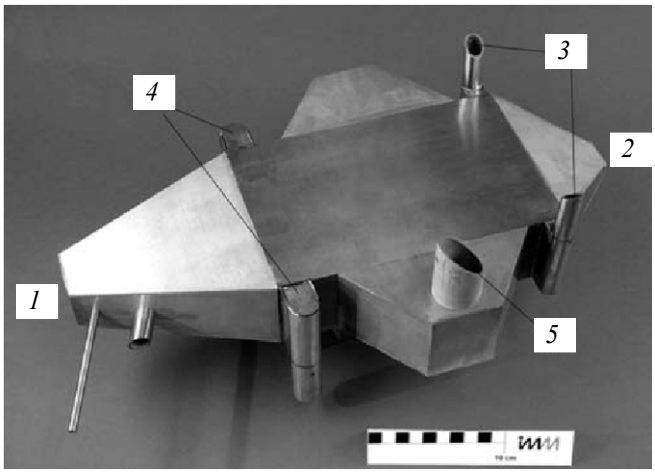

Fig. 3. Assembled single-stage microstructured reactor/heat-exchanger [67, 68]: (*1, 2*) inlet and outlet of the reaction mixture, respectively; (*3, 4*) inlet and outlet pipes for cooling gas; and (*5*) reactor preheating unit.

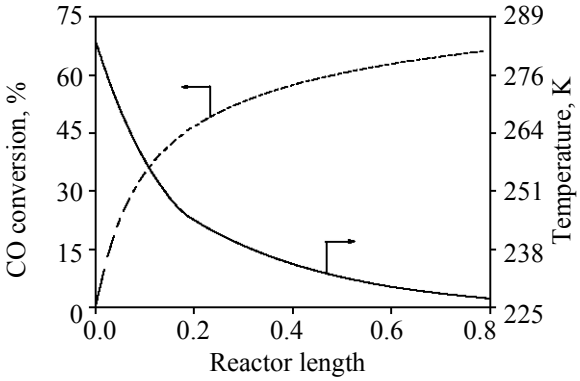

Fig. 4. Optimal temperature profile providing fast water–gas shift reaction in the 260–400 C and its corresponding CO concentration profile. Reaction conditions: p_{CO} 3.0 kPa, $p(H_2O)$ 27.0 kPa, $p(CO_2)$ 13.5 kPa, $p(H_2)$ 56.5 kPa; total flow rate 750 cm^3 min^{-1} (STP), Mo_2C weight 79.4 g.

7.6 kg. The reactor was tested at the following conditions: reaction flow rate 42.4 and 60.1 l min^{-1} at the CO concentrations 10.1 and 10.6 vol %, respectively; temperature decay along the reactor 410–250°C; heat flux from the reaction mixture to the cooling gas 96,15 W cm^{-2}, cooling gas flow rate 73 l min^{-1}. At lower and higher reaction flow rates, the CO conversion was 94 and 90 %, respectively, which corresponds to CO contents at the reactor outlet of 0.6 and 1.1 vol %, respectively.

Dubrovskiy et al. [66] proposed a microstructured reactor constructed of crimped and flat plates having channels with triangular cross sections. As known, microstructured reactors with triangular channels, assembled by alternating flat and crimped metal plates with a catalytic coating, have a high ratio of heat-exchange surface area to reactor internal volume. Their production cost is lower than that of reactors with heat-exchanger plates, having semi-cylindrical or triangular channels on both sides of the plate.

The space between crimped and flat plates was reduced by means of a molybdenum wire with the same catalytic coating as on the plates. Thus the "larger" triangular channel proved to be divided into three smaller channels with a geometry fairly exactly fitted by an equiangular triangle. Acute angles in a triangle-shaped channel affect the flow regime so that the average heat- and mass-transfer coefficients in the triangular channel are much lower than the respective parameters for cylindrical and rectangular channels. This has no impact on the efficiency of the reaction, since the water–gas shift reaction occurs fairly slowly in the temperature range 160–400°C and is kinetically controlled even in channels with a large hydraulic diameter. On the other hand, reduced thermal conductivity in the triangular channel can be compensated for by increased heat-exchange surface.

The digital calculations in [66] showed that the temperature profile in a countercurrent reactor/heat-exchanger can be adjusted so that it is ideal for the water–gas shift reaction. To this end, the device should be equipped with two additional side inlets for cooling gas.

The proposed construction offers a number of advantages over the two stage process.

The integrated reactor/heat-exchanger is more compact, its total internal volume is 1.5 times smaller compared to an isothermal reactor. The reaction occurs on one and the same catalyst encased in a single metal housing, which exclude the need in connection pipes, fittings, and other elements between two reactors.

In the course of the water–gas shift reaction which is an exothermic equilibrium reaction, the equilibrium concentration of CO decreases with temperature. As a result, a much higher performance can be reached at fairly high temperatures, when the composition of the gas mixture is far from equilibrium, with the subsequent temperature decrease, including the calculated optimal profile for the Mo_2C/Mo system [70] (Fig. 4).

Table 2. Principal parameters of the integrated reactor/heat-exchanger for the water–gas shift reaction [66]

Parameter	Value
Convective heat flux, W	
inlet	19.9
outlet	15.9
Reaction heat effect, W	0.50
Reaction-to-cooling channel heat transfer, W	4.50
Thermal conductivity of reaction material, W m^{-1} K^{-1}	16
Reactor cross-section, m^2	9.6×10^{-5}
Linear dimensions of the reactor, m	0.8×0.01×0.01
Reactor volume, m^3	8.0×10^{-5}
Weight of the Mo_2C coating in the reactor, g	74.9
Volume of the Mo_2C coating in the reactor, m^3	2.0×10^{-5}
Solid-phase fraction in the reactor (Mo_2C and Mo), %	74.6
Linear flow rate of the reaction mixture, m s^{-1}	0.492

A prototype reactor/heat-exchanger for the total flow of 750 ml min^{-1} and the outlet CO and H_2 concentrations of 1.0 and 58.0 vol %, respectively, which corresponds to the generation of 45 W of electric power in a fuel cell. This prototype heat-exchanger reactor is 1/22 part of a 1-kW fuel cell (this power can be reached by increasing the number of single modules) [66].

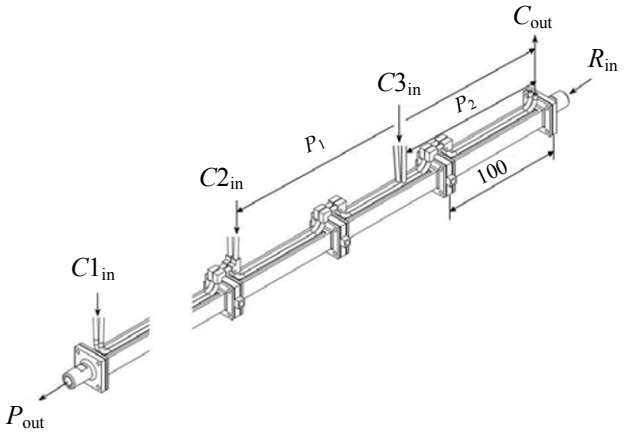

Fig. 5. Scheme of a microstructured reactor/heat-exchanger [66]: (C_{in}) inlet cooling gas flows; (C_{out}) total outlet cooling gas flow; (R_{in}, P_{out}) reagent and product flow, respectively; and (P_1, P_2) positions of additional channels for cooling gas injection.

Calculations using the kinetic database showed that for a 66 % conversion of CO in the developed reactor, 74.9 g of Mo_2C is required. The porous Mo_2C coating is formed on flat and crimped molybdenum plates and a molybdenum wire 250 μm in diameter by electrochemical deposition from salt melts.

The thermal conductivity of the material of the reactor and the cross-section of the latter define longitudinal heat transfer which can, provided the thermal conductivity of the reaction material is high enough, equalize the temperature inside the reactor. Moreover, there is a certain minimum reactor length which is capable of providing the necessary temperature gradient. The height of the reactor was made equal to its width (10 mm) to reduce the outer surface and, consequently, heat losses. The reactor material was AISI 316 stainless steel, an excellently corrosion-resistant and a low-cost material. The cross-section of a 10×10-mm^2 reactor with a 2-mm wall thickness is 9.6×10^{-5} m^2, which creates the thermal resistance of 650 K W^{-1} per 1 m reactor length. At the reaction length of 0.8 m (which ensures the required catalyst load) and the thermal conductivity coefficient of the reactor material of 16 W m^{-1} K^{-1}, the longitudinal heat flux comprises no more than 6% of 4.5 W, and this heat flux should be abstracted from the reaction channel to obtain the temperature gradient of 140°C. Such a temperature gradient provides a high heat recovery coefficient in the reactor/heat-exchanger. The principal parameters of this reactor/heat-exchanger are listed in Table 2.

The reactor comprises 8 sections, 0.105 m long each (Fig. 5). Each section contains 18 crimped and 17 flat Mo_2C/Mo plates and 288 Mo_2C/Mo wires. Each wire divides a "large" triangular channel into two smaller ones to form 576 triangular microchannels in each section of the microstructured reactor/heat-exchanger. The Mears criterion (relates to heat- and mass-transfer restrictions: when it is below 0.15, the restrictions are negligibly small) for the laminar flow in a tube is 0.006, and, therefore, no restrictions in external mass transfer are expected.

Thus, the integrated reactor/heat-exchanger allows to implement the water–gas shift reaction in one stage, which, in its turn, allows to reduce considerably the volume of the fuel processor.

ACKNOWLEDGMENTS

The work was financially supported by the Netherlands Organization for Scientific Research

(project no. 047.017.029) and Russian Foundation for Basic Research (project no. 047.011.2005.016).

REFERENCES

1. Ehrfeld, W., Hessel, V., and Löwe, H., *Microreactors: New Technologies for Modern Chemistry*, Weinheim: Wiley–VCH, 2000.
2. Löwe, H. and Ehrfeld, W., *Electrochim. Acta*, 1999, vol. 44, pp. 3679–3689.
3. Jensen, K.F., *Chem. Eng. Sci*., 2001, vol. 56, pp. 293–303.
4. Schubert, K., Bier, W., and Linder, G., *Chem. Ing. Tech*., 1989, vol. 61, pp. 172–173.
5. Ondrey, G., *Chem. Eng*., 1995, vol. 102, pp. 52–58.
6. Ehrfeld, W., Hessel, V., and Haverkamp, V., *Microreactors. in: Ullmann's Encyclopedia of Industrial Chemistry,* Weinheim: Wiley–VCH, 1999.
7. Gavriilidis, A., Angeli, P., Cao, E., Yeong, K.K., and Wan, Y.S.S., *Chem. Eng. Res. Des*., 2002, vol. 80, pp. 3–30.
8. Hessel, V., Hardt, S., and Löwe, H., *Chemical Micro Process Engineering*, Weinheim: Wiley–VCH, 2004.
9. Stankiewicz, A.I. and Moulijn, J.A., *Chem. Eng. Prog*., 2000, vol. 96, pp. 22–34.
10. Kestenbaum, H., Lange de Oliveira, A., Schmidt, W., Schoth, F., et al., *Ind. Eng. Chem. Res*., 2002, vol. 41, pp. 710–719.
11. Rebrov, E.V., Duinkerke, S.A., de Croon, M.H.J.M., and Schouten, J.C., *Chem. Eng. J*., 2003, vol. 93, pp. 201–216.
12. Kolb, G. and Hessel, V., *Ibid.*, 2004, vol. 98, pp. 1–38.
13. Knight, J.B., Vishwanath, A., Brody, J.P., and Austin, R.H., *Phys. Rev. Lett*., 1998, v.80, pp. 3863–3866.
14. Haswell, S.J., Middleton, R.J., O'Sullivan, B., Skelton, V., Watts, P., and Styring, P., *Chem. Commun*., 2001, pp. 391–398.
15. Besser, R.S., Ouyang, X., and Surangalikar, H., *Chem. Eng. Sci*., 2002, vol. 58, pp. 19–26.
16. Manz, A., Graber, N., and Widmer, H.M., *Sens. Actuators B*, 1990, vol. 1, pp. 244–248.
17. Zech, T. and Hőnicke, D., *Proc. Fourth Conf. on Microreaction Technology*, New York: AIChE, 2000, pp. 379–389.
18. Moller, A., Drese, K., Gnaser, H., Hampe, M., Hessel, V., Lowe, H., Schmitt, S., and Zapf, R., *Catal. Today*, 2003, vol. 81, pp. 377–391.
19. Hendershot, D.C., *Chem. Eng. Prog*., 2000, vol. 96, pp. 35–40.
20. Janicke, M., Holzwarth, A., Fichtner, M., Schubert, K., and Schoth, F., *Stud. Surf. Sci. Catal*., 2000, vol. 130, pp. 437–442.
21. Veser, G., *Chem. Eng. Sci*., 2001, vol. 56, pp. 1265–1273.
22. Benson, R.S. and Ponton, J.W., *Chem. Eng. Res. Des*., 1993, vol. 71, pp. 160–168.
23. Ajmera, S.K., Losey, M.W., and Jensen, K.F., *AIChE J*., 2001, pp. 1639–1647.
24. Hasebe, S., *Comput. Chem. Eng.,* 2004, pp. 57–64.
25. Worz, O., Jächel, K.-P., Richter, T., and Wolf, A., *Chem. Eng. Technol*., 2001, vol. 24, pp. 138–142.
26. Hogan, J., *Nature,* 2006, vol. 442, no. 7101, pp. 351–352.
27. Reisch, M., *Chem. Eng. News*, 2004, vol. 82, no. 35, p. 9.
28. Rouhi, A.M., *Ibid.*, 2004, vol. 82, no. 27, p. 18.
29. Freemantle M. *Ibid.*, 2004, vol. 82, no. 41, p. 39.
30. Luk'yanov, B.N., *Usp. Khim*., 2008, vol. 77, no. 11, pp. 1065–1087.
31. Rebrov, E.V., *Khim. Tekhnol*., 2009, vol. 10, no. 10, pp. 595–604.
32. Anxionnaz, Z., Cabassud, M., Gourdon, C., and Tochon, P., *Chem. Eng. Process*., 2008, vol. 47, pp. 2029–2050.
33. Kiwi-Minsker, L. and Renken, A., *Catal. Today*, 2005, vol. 110, pp. 2–14.
34. Gunardson, H., *Industrial Gases in Petrochemical Processing*, NewYork: Marcel Dekker, 1998.
35. Armor, J.N., *Appl. Catal. A*, 1999, vol. 176, pp. 159–176.
36. Ajmera, S.K., Delattre, C., Schmidt, M.A., and Jensen, K.F., *J. Catal*., 2002, vol. 209, pp. 401–412.
37. Menz, W., Mohr, J., and Paul, O., *Microsystem Technology*, Weinheim: Wiley–VCH, 2001, 2nd ed..
38. Belyaeva, N.P., *Katal. Prom-sti*, 2004, no. 2, p. 16.
39. Makarshin, L.L. and Parmon, V.N., *Ross. Khim. Zh*., 2006, vol. 50, no. 6, p. 19–25.
40. Andreev, A., Idakiev, V., Mihajlova, D., and Kunev, B., *React. Kinet. Catal. Lett*., 1986. vol. 33, pp. 119–124.
41. Edwards, M.A., Whittle, D.M., Rhodes, C., Ward, A.M., Rohan, D., Shannon, M.D., Hutchings, G. J., and Kiely, C., *J. Phys. Chem. Chem. Phys*., 2002, vol. 4, pp. 3902–3908.
42. Rhodes, C., Williams, B.P., King, F., and Hutchings, G., *J. Catal. Commun*., 2002, vol. 3, pp. 381–384.
43. Topsoe, H. and Boudart, M., *J. Catal*., 1973, vol. 31, pp. 346–359.
44. Lei, Y., Cant, N.W., and Trimm, D.L., *Chem. Eng. J*., 2005, vol. 114, pp. 81–85.
45. Liu, Q., Ma, W., He, R., and Mu, Z., *Catal. Today*, 2005, vol. 106, pp. 52–56.
46. Haruta, M*., Catal. Surv. Jpn*., 1997, vol. 1, pp. 61–73.
47. Burke, L.D. and Nugent, P.F., *Gold Bull*., 1998, vol. 31, pp. 39–51.

48. Bond, G.C., *Ibid.*, 2001, vol. 34, pp. 117–120.
49. Andreeva, D., *Ibid.*, 2002, vol. 35, pp. 82–88.
50. Ricote, S., Jacobs, G., Milling, M., Ji, Y., Patterson, P.M., and Davis, B.H., *Appl. Catal. A*, 2006, vol. 303, pp. 35–47.
51. Iida, H. and Igarashi, A., *Ibid.*, 2006, vol. 303, pp. 48–55.
52. Patt, J., Moon, D.J., Phillips, C., and Thompson, L., *Catal. Lett*., 2000, vol. 65, pp. 193–195.
53. Kim, H.-G., Lee, K. H., and Lee, J. S., *Res. Chem. Intermed*., 2000, vol. 26, pp. 427–443.
54. Moon, D.-J. and Ryu, J.W., *Catal. Lett*., 2004, vol. 92, pp. 17–24.
55. US Patent 6623720, 2003.
56. LaMont, D.C, Gilligan, A.J., Darujati, A.R.S., Chellappa, A.S., and Thomson, W. J., *Appl. Catal. A*, 2003, vol. 255, pp. 239–255.
57. Darujati, A.R.S., LaMont, D.C., and Thomson, W.J., *Ibid.*, 2003, vol. 253, pp. 397–407.
58. Zhu, Q., Zhang, B., Zhao, J., Ji, S., Yang, J., Wang, J., and Wang, H., *J. Mol. Catal. A*, 2004, vol. 213, pp. 199–205.
59. Floquet, N., Bertrand, O., and Heizmann, J.J., *Oxid. Met*., 1992, vol. 37, pp. 253–280.
60. Kuznetsov, S.A., Dubrovskiy, A.R., Rebrov, E.V., and Schouten, J.C., *Z. Naturforsch*., 2007, vol. 62a, pp. 647–654.
61. Dubrovskii, A.R., Kuznetsov, S.A., Rebrov, E.V., and Schouten, J.C., *Kinet. Katal*., 2008, vol. 49, no. 4, pp. 620–624.
62. Dubrovskii, A.R., Kuznetsov, S.A., Rebrov, E.V., Schouten, J.C., and Kalinnikov, V.T., *Dokl. Akad. Nauk*, 2008, vol. 421, no. 6, pp. 769–772.
63. Tonkovich, A.Y., Zilka, J.L., La Mont, M.J., Wang, Y., and Wegeng, R.S., *Chem. Eng. Sci*., 1999, vol. 54, pp. 2947–2951.
64. Goerke, O., Pfeifer, P., and Schubert, K., *Appl. Catal. A*, 2004, vol. 263, no. 1, pp. 11–18.
65. Kolb, G., Schurer, J., Tiemann, D., Wichert, M., Zapf, R., Hessel, V., and Lowe, H., *J. Power Sources*, 2007, vol. 171, no. 1, pp. 198–204.
66. Dubrovskiy, A.R., Rebrov, E.V., Kuznetsov, S.A., and Schouten, J.C., *Catal. Today*, 2009, vol. 147, no. 1, pp. S198–S203.
67. Kolb, G., Hofmann, C., O'Connell, M., and Schurer, J., *Ibid.*, 2009, vol. 147, no. 1, pp. 176–184.
68. O'Connell, M., Kolb, G., Schelhaas, K.P., Schuerer, J., Tiemann, D., Ziogas, A., and Hessel, V., *Int. J. Hydrogen Energ*., 2010, vol. 35, no. 6, pp. 2317–2327.
69. Kolb, G., Baier, T., Schurer, J., Tiemann, D., Ziogas, A., Specchia, S., Galletti, C., Germani, G., and Schuurman, Y., *Chem. Eng. J*., 2008, vol. 138, nos. 1–3, pp. 474–489.
70. Rebrov, E.V., Kuznetsov, S.A., de Croon, M.H.J.M., and Schouten, J.C., *Catal. Today*, 2007, vol. 125, pp. 88–96.